Unified theory of second sound in two-dimensional materials

Man-Yu Shang,[1] Wen-Hao Mao,[1] Nuo Yang,[2] Baowen Li,[3,4,*] and Jing-Tao Lü[1,†]

[1]*School of Physics and Wuhan National High Magnetic Field Center, Huazhong University of Science and Technology, 430074 Wuhan, P. R. China*

[2]*School of Energy and Power Engineering, Huazhong University of Science and Technology, 430074 Wuhan, P. R. China*

[3]*Department of Material Science and Engineering, Department of Physics, Shenzhen Institute for Quantum Science and Engineering, Southern University of Science and Technology, Shenzhen 518055, China*

[4]*Paul M. Rady Department of Mechanical Engineering and Department of Physics, University of Colorado, Boulder, Colorado 80305-0427, USA*

(Received 15 July 2021; revised 27 January 2022; accepted 8 April 2022; published 21 April 2022)

We develop a unified theory for second sound in two-dimensional materials. Previously studied drifting and driftless second sound are two limiting cases of the theory, corresponding to the drift and diffusive part of the energy flux, respectively. We find that due to the presence of quadratic flexural phonons, the drifting second sound does not exist in the thermodynamic limit, while the driftless mode is less affected. This is understood as a result of infinite effective inertia of flexural phonons, due to their constant density states and divergent Bose-Einstein distribution in the long wavelength limit. Consequently, the group velocity of the drifting mode is smaller than that of the driftless mode. However, upon tensile strain, the velocity of the drifting mode becomes larger. Both of them increase with tensile strain due to the linearization of the flexural phonon dispersion. Our results clarify several puzzles encountered previously and pave the way for exploring wavelike heat transport beyond the hydrodynamic regime.

DOI: 10.1103/PhysRevB.105.165423

I. INTRODUCTION

While the diffusive Fourier heat conduction is ubiquitous in bulk solids, the violation in various circumstances, in particular in low dimensional systems, has been observed and is becoming a strong focus of current research in condensed matter and statistical physics, nanomaterial science, and engineering [1–6]. One example of such a violation is the wavelike propagation of temperature field (Fig. 1), termed second sound, an emergent many-body phenomenon resulting from frequent phonon scattering [7–13]. Thermal wave transport provides new opportunities for heat management, information processing, and novel device applications [4,5,14–16]. Exploring its role in anomalous thermal transport may offer new insight into the divergent thermal conductivity of a low dimensional system [3–6]. Early research has led to observation of second sound only in a handful of materials [17–27]. Recent progress on phonon [28–44] and electron [45–51] hydrodynamic transport in two-dimensional (2D) materials has triggered its renewed interest, based on which coupled electron-phonon hydrodynamics has been anticipated [52–54]. However, direct experimental observation of phonon second sound and its connection with anomalous thermal conductivity in 2D materials is still lacking.

Theoretical analysis has identified two types of second sound, denoted as drifting and driftless modes, respectively [23]. The drifting mode exists in the hydrodynamic transport regime, where crystal momentum conservation is approximately fulfilled during phonon scattering. This requires the momentum-conserving normal scattering (N scattering) process to dominate over the nonconserving processes (R scattering). The latter includes Umklapp scattering, impurity scattering, and scattering with other quasiparticles. The existence of the driftless mode requires that the heat-carrying phonons have similar relaxation time, which should be much longer than the inverse of external driving frequency. Its existence does not rely on the hydrodynamic conditions and is possible even in the diffusive regime. Although these two types of second sound have been noticed a long time ago [23,55], their different nature has not been clarified, leaving the experimentally observed second sound in different materials unclassified [34,56]. Moreover, in the two seminal works on 2D materials [28,29], to avoid an infrared divergence introduced by the quadratic flexural phonons, two different expressions for the second sound velocity have been used, which needs further clarification.

By combining momentum and energy flux balance equations, we develop a unified theory to understand the nature of phonon second sound in 2D materials. We show that the drifting and driftless modes emerge in our theory as two limiting cases, and they are rooted in the drift and diffusive part of the total energy flux, corresponding to the first and second terms on the right-hand side (rhs) of Eq. (6), respectively. More importantly, in ideal nonstrained 2D materials, the constant density of states of quadratic flexural phonons and divergent Bose-Einstein distribution in the long wavelength limit together give rise to logarithmic divergence of the phonon number density with system size. Consequently, the drifting second sound does not exist in the thermodynamic limit. This is a common feature of bosonic quasiparticles with quadratic

*libw@sustech.edu.cn
†jtlu@hust.edu.cn

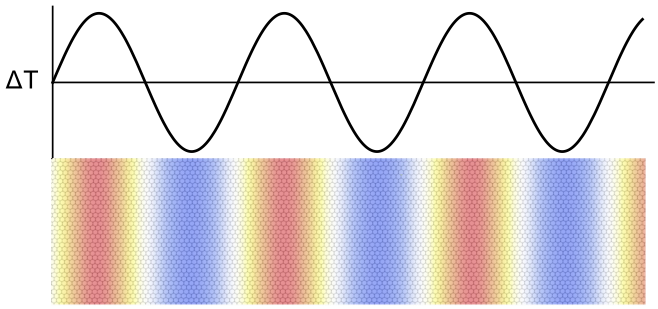

FIG. 1. Schematic diagram of second sound propagation.

dispersion but without number conservation, and reveals the physical origin of the infrared divergence encountered in previous works [28,29,36,38,57].

II. THEORY

A. Balance equations

We follow a kinetic approach and employ the Peierls-Boltzmann equation in the Callaway approximation to describe the phonon transport [58],

$$\frac{\partial f_{i\boldsymbol{k}}}{\partial t} + \boldsymbol{v}_{i\boldsymbol{k}} \cdot \nabla f_{i\boldsymbol{k}} = -\frac{f_{i\boldsymbol{k}} - f_{R,i\boldsymbol{k}}}{\tau_{R,i\boldsymbol{k}}} - \frac{f_{i\boldsymbol{k}} - f_{N,i\boldsymbol{k}}}{\tau_{N,i\boldsymbol{k}}}. \tag{1}$$

Here $\tau_{R,i\boldsymbol{k}}$ and $\tau_{N,i\boldsymbol{k}}$ are two mode-resolved, $\boldsymbol{k}$-dependent relaxation times introduced to describe R and N processes, respectively. $f_{i\boldsymbol{k}}$ is the nonequilibrium phonon distribution, $\boldsymbol{v}_{i\boldsymbol{k}}$ is the phonon group velocity, and i is the phonon branch index. Hereafter we omit $i\boldsymbol{k}$ for brevity when there is no ambiguity. It is known that with R scattering the system relaxes to the Bose-Einstein distribution

$$f_{R,i\boldsymbol{k}} = \{\exp[\beta\hbar\omega_{i\boldsymbol{k}}] - 1\}^{-1}, \tag{2}$$

where $\hbar$ is the reduced Planck constant, $\omega_{i\boldsymbol{k}}$ is the phonon angular frequency, and $\beta = (k_B T)^{-1}$ is the inverse temperature with the Boltzmann constant k_B and the absolute temperature T. Meanwhile, in the presence of only N scattering, the system relaxes instead to a drifted Bose-Einstein distribution

$$f_{N,i\boldsymbol{k}} = \{\exp[\beta(\hbar\omega_{i\boldsymbol{k}} - \hbar\boldsymbol{k}\cdot\boldsymbol{u})] - 1\}^{-1}, \tag{3}$$

with a characteristic drift velocity $\boldsymbol{u}$ common to all phonon modes.

The balance equations can then be derived by considering the (quasi-)conserved quantities in the kinetics. Since phonons represent thermal excitation of the atomic motion, their number is not a conserved quantity. Thus, we are left only with energy and crystal momentum,

$$\partial_t E + \nabla \cdot \boldsymbol{q} = 0, \tag{4}$$

$$\partial_t \boldsymbol{p} + \nabla \cdot \boldsymbol{\Phi} = -\langle \tau_R^{-1} \rangle_p \boldsymbol{p}, \tag{5}$$

E and $\boldsymbol{p}$ are the energy and momentum density, and $\boldsymbol{q}$ and $\boldsymbol{\Phi}$ are the corresponding fluxes. The averaged inverse relaxation time $\langle \tau_R^{-1} \rangle_p$ [Eq. (A4a)] characterizes the relaxation of $\boldsymbol{p}$ due to R scattering. The energy conservation results from ignoring scattering processes that transfer energy to other quasiparticles, i.e., electrons. We also need an equation for the energy flux $\boldsymbol{q}$,

$$\langle \tau_c \rangle_q \partial_t \boldsymbol{q} + \boldsymbol{q} = \chi W^{(0)} \boldsymbol{u} - \boldsymbol{\kappa} \cdot \nabla T. \tag{6}$$

The total energy flux includes two contributions. The first term on the rhs is due to the collective phonon drift motion, while the second is due to a temperature gradient. Here $\langle \tau_c \rangle_q$ [Eq. (A24)] is a characteristic relaxation time of $\boldsymbol{q}$, κ [Eq. (A26)] is the thermal conductivity in the relaxation time approximation, $W^{(0)}$ [Eq. (A9)] is the enthalpy function evaluated by approximating $f_{i\boldsymbol{k}} \approx f^{(0)}_{i\boldsymbol{k}} = f_{N,i\boldsymbol{k}}$, and χ [Eq. (A25)] is an averaged dimensionless parameter characterizing the relative contribution of N scattering to the total scattering rate. Details of the derivation and the definition of these variables can be found in Appendix A.

B. Linear phonons

We start by considering a single phonon branch with linear dispersion, where the energy flux and the momentum density are simply proportional to each other, i.e., $\boldsymbol{q} = v_g^2 \boldsymbol{p}$. To linear order in u, we have $\boldsymbol{q} = W^{(0)} \boldsymbol{u}$. This holds for "relativistic" quasiparticles with linear dispersion. Using this equivalence, a Guyer-Krumhansl equation can be derived [21,22,59]. Combining with Eq. (4), we can get a wave solution for the temperature field, with group velocity $v = v_g/\sqrt{D}$, where D is the system dimension and v_g is the phonon group velocity (see also Appendix C).

We can use this simple case to make a connection with second sound in helium II (Appendix C). The common drift velocity $\boldsymbol{u}$ here plays the role of relative velocity between the normal and superfluid in helium II. Both of them are sustained even in the absence of external driving, carrying no entropy, and are essential for propagation of second sound. However, they are from different microscopic origin. Here, it requires frequent momentum-conserving N scattering to sustain the collective drift motion, while in helium it relies on Bose-Einstein condensation to produce superfluid helium and its relative motion with the normal fluid.

In the presence of more phonon branches, i.e., longitudinal and transverse acoustic branches, having different group velocity $v_{g,i}$, the proportionality between $\boldsymbol{p}$ and $\boldsymbol{q}$ does not hold, giving rise to the drifting and driftless second sound with their velocity [55]

$$v_p \approx \sqrt{\left(\sum_i v_{g,i}^{-D}\right) \Big/ \left(D \sum_i v_{g,i}^{-(D+2)}\right)} \tag{7}$$

and

$$v_q \approx \sqrt{\sum_i v_{g,i}^{2-D} \Big/ \left(D \sum_i v_{g,i}^{-D}\right)}, \tag{8}$$

respectively [60]. The situation changes qualitatively in the presence of flexural phonons with quadratic dispersion.

C. Flexural phonons

In the ideal, nonstrained 2D system, the flexural phonons have quadratic dispersion with constant density of states. The large Grüneisen parameter indicates their dominant role in

the anharmonic N scattering. This has been attributed to the physical mechanism leading to phonon hydrodynamics in a much wider temperature range in 2D materials [28]. However, the quadratic distribution poses difficulties in the traditional kinetic theory treatment of phonon hydrodynamics, where a small-u expansion on $f_{N,i\boldsymbol{k}}$ is performed, i.e.,

$$f_N \approx f_R + \beta f_R(f_R+1)\hbar\boldsymbol{k}\cdot\boldsymbol{u}. \tag{9}$$

Unfortunately this expansion fails for $\hbar\omega_{i\boldsymbol{k}} \sim \hbar\boldsymbol{k}\cdot\boldsymbol{u}$, which is always true for a quadratic dispersion in the long wavelength limit. More severe is the unphysical case when $\hbar\omega_{\boldsymbol{k}} < \hbar\boldsymbol{k}\cdot\boldsymbol{u}$ and $f_{\boldsymbol{k}} < 0$. This has been the main obstacle in understanding 2D phonon hydrodynamics and in applying a fully numerical approach to realistic materials [57].

To focus on this problem, we postpone the full analysis and consider the flexural phonon branch only. We derive the hydrodynamic equation using the full form of f_N instead. We furthermore introduce an effective mass $m^* = \hbar/2a$ for the flexural phonons, such that

$$\hbar\omega_k = \hbar a k^2 = \hbar^2 k^2/2m^*. \tag{10}$$

Note that m^* is introduced for notational convenience and is not the atomic mass. We can then derive a generalized Euler equation from Eq. (5) (Appendix A),

$$(\partial_t + \boldsymbol{u}\cdot\boldsymbol{\nabla})\boldsymbol{u} + (\boldsymbol{\nabla}\cdot\boldsymbol{u})\boldsymbol{u} + \boldsymbol{\nabla}P^{(0)}/\rho_N^{(0)} = -\left\langle\tau_R^{-1}\right\rangle_p\boldsymbol{u}. \tag{11}$$

Here $P^{(0)}$ is the effective pressure of the phonon gas [Eq. (A10b)], and $\rho_N^{(0)} = n_N^{(0)}m^*$ is the effective mass density, with the phonon number density $n_N^{(0)} = L^{-2}\sum_{\boldsymbol{k}} f_{N,\boldsymbol{k}}$. With these effective parameters, Eq. (11) takes the standard form for nonrelativistic particles [61].

To consider wave solutions, we ignore terms nonlinear in $\boldsymbol{u}$. One important feature of flexural phonons is that $\rho_N^{(0)}$ diverges logarithmically with system size L,

$$\rho_N^{(0)}(u=0) \propto \ln L. \tag{12}$$

This is due to their constant density of states at $k = 0$ where $f_{R,\boldsymbol{k}}$ diverges. The divergent $\rho_N^{(0)}$ results in an equation about $\boldsymbol{u}$ as $\partial_t\boldsymbol{u} = -\langle\tau_R^{-1}\rangle_p\boldsymbol{u}$, with the steady-state solution $\boldsymbol{u} = 0$. Thus, we reach one important result: the quadratic flexural phonons do not support the drifting second sound in the thermodynamic limit. Consequently, the problem with negative occupation $f_{\boldsymbol{k}} < 0$ does not occur. This is a general feature of 2D bosonic quasiparticles with quadratic dispersion that lack number conservation. We have provided an intuitive explanation of this result as a consequence of their infinite effective inertia.

Considering instead the energy flux, we obtain a damped wave solution for the driftless second sound with velocity

$$v_q \approx \sqrt{\kappa/\left(C_N^{(0)}\langle\tau_c\rangle_q\right)}. \tag{13}$$

It depends on the heat capacity of flexural phonons $C_N^{(0)}$, instead of the divergent $\rho_N^{(0)}$.

The existence of driftless sound mode can be understood as follows. When a time dependent external temperature gradient is applied to the system, the energy current response is also time dependent. The finite response time of the system is taken into account by the first term in Eq. (6). In the case $\langle\tau_c\rangle_q\partial_t\boldsymbol{q} \gg \boldsymbol{q}$, Eqs. (4) and (6) allow damped wave solutions. This situation is similar to the optical response of free electrons in the Drude model. We get a frequency-dependent thermal conductivity [21,62–65]

$$\kappa(\omega) = \frac{\kappa}{1 - i\omega\langle\tau_c\rangle_q}. \tag{14}$$

The real part represents in-phase response of $\boldsymbol{q}$ to the time dependent temperature field, resulting in dissipation, while the imaginary part has a $\pi/2$ phase lag and gives rise to wave propagation. It becomes dominant for $\omega \gg \langle\tau_c\rangle_q^{-1}$. This means that the existence of the driftless second sound does not rely on the stringent phonon hydrodynamic conditions, but requires a high frequency excitation. Recent experimental observation of second sound under high frequency excitation in Ge seems to fall into this regime [56].

D. Full analysis

We now turn to the full form of the balance equations by including two linear and one flexural acoustic branches. We furthermore include the viscous dissipation, which generates damping of second sound. Correspondingly, the generalized Euler equation is modified to a Navier-Stokes equation (Appendix A)

$$\begin{aligned}(\partial_t + \boldsymbol{u}\cdot\boldsymbol{\nabla})\boldsymbol{u} + (\boldsymbol{\nabla}\cdot\boldsymbol{u})\boldsymbol{u} \\ = -\boldsymbol{\nabla}P^{(0)}/\rho^{(0)} + \eta/\rho^{(0)}\nabla^2\boldsymbol{u} + \xi/\rho^{(0)}\boldsymbol{\nabla}(\boldsymbol{\nabla}\cdot\boldsymbol{u}) - \left\langle\tau_R^{-1}\right\rangle_p\boldsymbol{u}.\end{aligned} \tag{15}$$

The bulk (η) and shear (ξ) viscosity coefficients describes the hydrodynamic dissipation, with $\xi = 0$ in 2D (Appendix B), and $\rho^{(0)}$, $P^{(0)}$ include contributions from all phonon branches. We note that all the zeroth order quantities are evaluated using f_N, instead of the thermal equilibrium f_R. This is different from the standard relativistic and nonrelativistic hydrodynamics. Consequently, phonons do not fulfill the Lorentz or Galilean invariance [54]. Only when we consider second sound propagation and keep only terms linear in u, can they be recovered (Appendix A 2 e). In that case, considering small deviations of $\boldsymbol{u}$, T and $\boldsymbol{q}$ on top of their equilibrium value with the form

$$\boldsymbol{u}, \delta T, \delta\boldsymbol{q} \propto \exp(-i\omega t + i\boldsymbol{k}\cdot\mathbf{r}), \tag{16}$$

we obtain a set of linear equations from Eqs. (4), (6),and (15),

$$\begin{pmatrix} \omega & 0 & -k_\alpha/C^{(0)} \\ -k_\alpha C_P^{(0)}/\rho^{(0)} & \omega + i\left\langle\tau_R^{-1}\right\rangle_p + i(\eta+\xi)k_\alpha^2/\rho^{(0)} & 0 \\ ik_\alpha\kappa & -\chi W^{(0)} & 1 - i\omega\langle\tau_c\rangle_q \end{pmatrix}\begin{pmatrix}\delta T \\ u_\alpha \\ \delta q_\alpha\end{pmatrix} = 0, \tag{17}$$

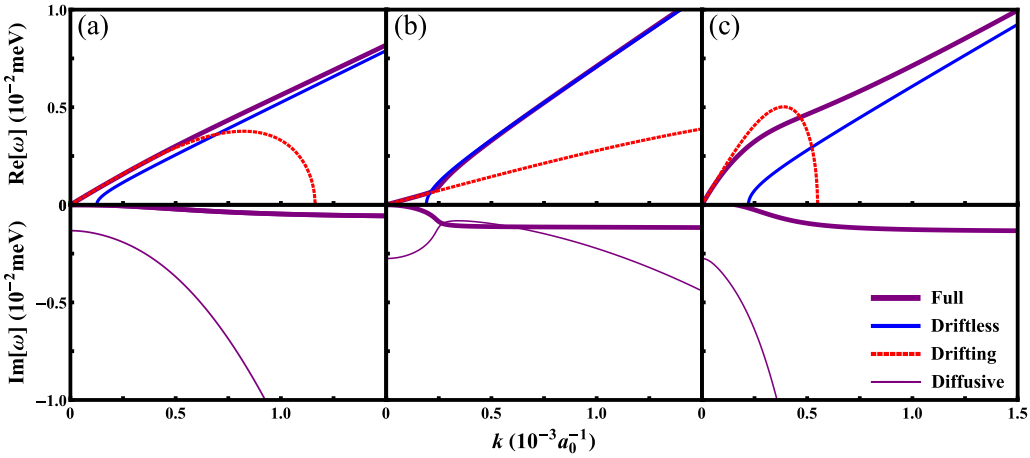

FIG. 2. The second sound dispersion relation of graphene calculated using parameters obtained from DFT calculations at $T = 100$ K shown in Figs. 5–7. We take $L = 50$ μm, corresponding to a low cutoff wave vector $k_{\rm cut} \sim 3 \times 10^{-5} a_0^{-1}$, where $a_0 = 2.47$ Å is the lattice constant of graphene. The red dashed and blue solid lines correspond to solutions of the drifting and driftless modes, while the purple lines are the full solutions [Eq. (17)]. The drifting modes are calculated by taking $\boldsymbol{q} = W^{(0)}\boldsymbol{u}$, while the driftless modes are obtained by taking $\boldsymbol{u} = 0$ in Eq. (17). The upper and lower panel give the real and imaginary parts, respectively. Only positive solutions are shown in the upper panel, while only the full solutions are shown in the lower. In the lower panel, the absolute value of the thick line gives the lifetime of the second sound in the upper panel, while the thin line is the diffusive mode with a zero real part. Thus, the actual heat transport composes both the sound and the diffusive mode simultaneously. In (a) the force constants from DFT calculations are used directly, while in (b) additional rotational symmetry is applied to the force constants. In (c) the flexural phonons are excluded.

where $C_P^{(0)} = \partial P^{(0)}/\partial T$, $\alpha = x, y, z$. Dispersion relations of the associated modes can be obtained from the condition $\det A = 0$, where A is the 3×3 matrix in Eq. (17).

Before presenting the numerical result, we can show that the drifting and driftless modes show up as two limiting cases of Eq. (17). In the first limit, when the drifting part dominates, the energy flux $\boldsymbol{q} \approx \boldsymbol{q}^{(0)} = W^{(0)}\boldsymbol{u}$. Equation (17) gives

$$\omega_p(k) \approx \pm \sqrt{\frac{W^{(0)}\left(\sum_i \alpha_i C_i^{(0)}\right)}{\rho^{(0)} C^{(0)}} k^2 - \frac{1}{4}\delta^2(k)} - \frac{i}{2}\delta(k), \quad (18)$$

with $\delta(k) = \langle \tau_R^{-1} \rangle_p + (\eta + \xi)k^2/\rho^{(0)}$ (red dashed lines in Fig. 2). The coefficient $\alpha_L = 1/2$ for linear mode and $\alpha_N = 1$ for quadratic flexural mode. $\rho^{(0)}$ in the denominator indicates their origin from the momentum balance equation. Since $\rho_N^{(0)}$ diverges as $\ln L$ in the thermodynamic limit, there is no drifting second sound solution. In the other limit, when the angular frequency is much larger than the inverse decay time of the energy flux $\omega \gg \langle \tau_c \rangle_q^{-1}$, there can still be a wave solution even when $u = 0$. We get the driftless sound mode

$$\omega_q(k) = \pm \sqrt{\frac{\kappa}{C^{(0)}\langle \tau_c \rangle_q} k^2 - \frac{\langle \tau_c \rangle_q^{-2}}{4}} - \frac{i}{2}\langle \tau_c \rangle_q^{-1}, \quad (19)$$

which are mainly associated with the second term on the rhs of Eq. (6) (blue solid lines in Fig. 2).

We note that, in practice, several factors can lead to a finite $\rho_N^{(0)}$ and consequently a slow drifting second sound. First, the finite size of the sample introduces a low cutoff to the wave vector $k_{\rm cut} \sim 2\pi/L$, where L is the length of the 2D sample. Second, it is known that the low frequency flexural mode in 2D materials is strongly anharmonic, which may lead to a renormalized dispersion $\omega_k \propto k^\gamma$ with $1 < \gamma < 2$ [66] (see however Ref. [67] for an opposite view), removing the divergence in $n_N^{(0)}$. Third, tensile strain can harden the flexural mode and introduce a linear dispersion near $k = 0$. Notably, although in practice the divergence can be avoided, the drifting second sound velocity can be drastically reduced by the quadratic dispersion of flexural mode (Fig. 2).

III. NUMERICAL RESULTS

We now turn to fully numerical calculations. Figure 2 presents the dispersion relation obtained by solving Eq. (17) numerically, where only the positive solution is shown (purple solid lines). We use realistic parameters obtained from density functional theory (DFT) calculations of graphene (details in Appendix D). To study the drifting mode, we have chosen a cut-off wave vector corresponding to a finite size system with $L = 50$ μm. Similar results are obtained for single layer boron nitride (not shown here).

The drifting mode (red dashed line) exists in the long wavelength limit with the upper cutoff determined by the condition $\omega_p(k) \approx \delta(k)/2$ [Eq. (18)]. On the other hand, the driftless mode (blue solid) has a lower cutoff determined by $\omega_q(k) \approx \langle \tau_c \rangle_q^{-1}/2$ [Eq. (19)]. These two limiting wave vectors determine the overlap regime of the two types of second sound. The ideal quadratic dispersion of flexural phonons is not guaranteed from the numerical force constants. Additional symmetrization is applied to recover the quadratic dispersion [68]. Figures 2(a) and 2(b) show the resulting second sound dispersion before and after the symmetrization. A clear transition from drifting to driftless mode is observed in Fig. 2(b), but is difficult to see in Fig. 2(a). This shows that a small deviation from quadratic dispersion can lead to a large change in the second sound dispersion. Figure 2(c) shows the dispersion excluding flexural phonons. Comparing Figs. 2(b) and 2(c) we find that inclusion of flexural phonons drastically reduces

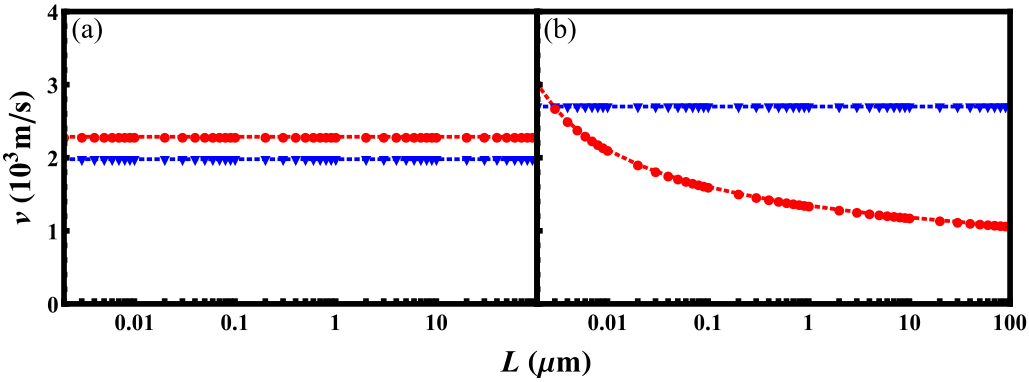

FIG. 3. Size (L) dependence of drifting (red circle) and driftless (blue triangle) second sound velocities before (a) and after (b) applying the rotational symmetry.

the velocity of the drifting mode. Notably, in the two seminal papers on second sound in graphene, Ref. [28] considered the drifting mode, while Ref. [29] considered the driftless mode.

Figure 3 shows the length dependence of the drifting (red) and driftless (blue) second sound velocity. Before the symmetrization, both modes show size-independent group velocity. The reduction of drifting mode velocity due to increasing $\rho_N^{(0)} \propto \ln L$ is observed for ideal quadratic phonon dispersion. This indicates that the logarithmic divergence of $\rho_N^{(0)}$ or length dependence of v_p is easily destroyed by a small deviation from an ideal quadratic dispersion in the numerical calculations. This may explain the reason why convergent results can be obtained in previous numerical results [28,38].

Since tensile strain can introduce a linear part to the dispersion to flexural phonons, we have plotted how it changes the velocity of drifting and driftless second sound in Fig. 4. Both of them increase with applied strain. This can be attributed to the increasing group velocity of flexural phonons with strain (inset). It is a special feature of 2D materials with flexural phonons and is, in principle, observable in experiments.

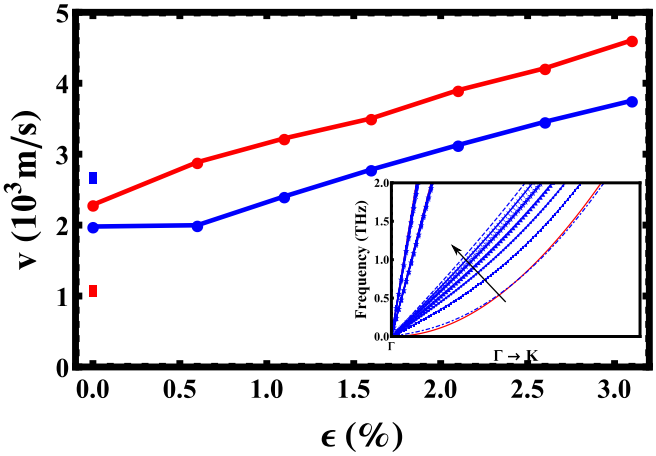

FIG. 4. Dependence of drifting (red) and driftless (blue) second sound velocity v on the applied tensile strain $\epsilon = (a - a_0)/a_0$ for $L = 50$ μm. The rectangular dots at $\epsilon = 0$ are the results after applying rotational symmetry. In the inset, the red solid line shows the dispersion of flexural mode after symmetrization. The blue lines show how the dispersion changes with increasing tensile strain from 0% to 3.1% in the arrow direction. Hardening of the flexural mode with tensile strain is observed, while the transverse and longitudinal acoustic modes are less affected.

Finally, we discuss implication of these results on the thermal conductivity of 2D materials. The presence of drift motion in Eq. (6) generally results in larger thermal conductivity than that obtained from relaxation time approximation [58]. This has been used as one signature of hydrodynamic transport [29,69]. For sufficiently weak damping, the collective drift motion is sustained and the thermal conductivity may diverge. Our analysis here suggests that ideal quadratic dispersion of flexural phonons suppresses the drift motion in the long wavelength limit. On the other hand, it has been predicted that thermal conductivity of 2D materials diverges logarithmically with system size. This has been supported both by numerical calculations [70–76] and experimental measurement [77]. Numerical simulations further suggest that divergent thermal conductivity emerges once there is small linear contribution to the flexural phonon dispersion. This seems inline with our prediction that drifting second sound emerges in the thermodynamic limit under the same condition. However, it has been shown [71,76] that thermal conductivity diverges even when the Boltzmann equation is solved under relaxation time approximation in which case hydrodynamic transport is absent. Thus, we argue that hydrodynamic phonon transport is not a necessary condition for divergent thermal conductivity.

IV. CONCLUSIONS

We have clarified the role of flexural phonons in 2D materials on the propagation of drifting and driftless second sound by developing a theory that takes both into account under equal footing. In addition to providing enlarged N-scattering phase space, an infinite effective inertial effect of flexural phonons, logarithmically divergent with system size, destroys the propagation of drifting second sound in the thermodynamic limit. On the other hand, the driftless second sound is less affected. We suggest that propagation of high frequency driftless second sound is possible even in the diffusive system and may have been experimentally observed [56]. This greatly extends the scope of materials where wavelike heat transport can be explored.

ACKNOWLEDGMENTS

We thank Wu Li for assistance in recovering ideal quadratic dispersion of flexural phonons. We acknowledge funding support from National Natural Science Foundation of China (Grant No. 21873033), the National Key Research and Development Program of China (Grant No. 2017YFA0403501), and the program for HUST academic frontier youth team. The computing resources are provided by Shanghai supercomputer center.

APPENDIX A: DERIVATION OF THE HYDRODYNAMIC EQUATIONS

1. Kinetic equation and conservation laws

We consider a generalized Debye model to include the flexural phonons with quadratic dispersion $\omega_k = ak^2$, in additional to the linear mode $\omega_k = v_g k$. We define an effective mass $m^* = \hbar/(2a)$, so that the energy of flexural phonons can be written as $\hbar\omega_k = \hbar^2 k^2/(2m^*)$. This form resembles that of nonrelativistic particles. Correspondingly, phonons with linear dispersion could be thought as relativistic quasiparticles.

To describe phonon transport in the system, we start from the Peierls-Boltzmann equation in the Callaway approximation [Eq. (1)]. Following the standard approach, we get the respective balance equations for energy and momentum density given in Eqs. (4) and (5). The 2D energy (E) and momentum ($\boldsymbol{p}$) density are defined as

$$E = L^{-2}\sum_{ik}\hbar\omega_{ik}f_{ik} = \sum_i E_i, \tag{A1a}$$

$$\boldsymbol{p} = L^{-2}\sum_{ik}\hbar\boldsymbol{k}f_{ik} = \sum_i \boldsymbol{p}_i, \tag{A1b}$$

while $\boldsymbol{q}$ and $\boldsymbol{\Phi}$ are their flux densities

$$\boldsymbol{q} = L^{-2}\sum_{ik}\hbar\omega_{ik}\boldsymbol{v}_{ik}f_{ik} = \sum_{ik}\boldsymbol{q}_{ik}, \tag{A2}$$

$$\boldsymbol{\Phi} = L^{-2}\sum_{ik}\hbar\boldsymbol{k}\boldsymbol{v}_{ik}f_{ik} = \sum_{ik}\boldsymbol{\Phi}_{ik}. \tag{A3}$$

Here L^2 is the area of the sample. We have introduced an averaged relaxation time defined as

$$\langle\tau_R^{-1}\rangle_p = \frac{\sum_{ik}\tau_{R,ik}^{-1}\hbar\boldsymbol{k}(f_{ik}-f_{R,ik})}{\sum_{ik}\hbar\boldsymbol{k}(f_{ik}-f_{R,ik})}, \tag{A4a}$$

$$\langle\tau_N^{-1}\rangle_p = \frac{\sum_{ik}\tau_{N,ik}^{-1}\hbar\boldsymbol{k}(f_{ik}-f_{N,ik})}{\sum_{ik}\hbar\boldsymbol{k}(f_{ik}-f_{N,ik})}. \tag{A4b}$$

We have $\langle\tau_N^{-1}\rangle_p = 0$ due to crystal-momentum conservation. These averages are different, which is a manifestation of the fact that the same scattering process may relax physical quantities with different efficiency.

2. Zeroth order approximation and Euler equation

We follow the standard approach in deriving the hydrodynamic equations [36,59,61]. In the zeroth order approximation, the distribution function is approximated by

$$f \approx f^{(0)} = f_N. \tag{A5}$$

This applies when N-scattering process is much stronger than R scattering. In the following, to derive the zeroth order physical quantities, we use the full form of f_N instead of the commonly used expansion $f_N \approx f_R + \beta f_R(f_R+1)\hbar\boldsymbol{k}\cdot\boldsymbol{u}$. The small-$u$ limit can be taken afterwards based on the full results. This is the main difference between present work and most of the previous studies. We will show that this is convenient to understand the divergence encountered when dealing with flexural phonons. In order to get closed expressions, we make the following approximation for the summation over $\boldsymbol{k}$:

$$L^{-2}\sum_{\boldsymbol{k}} f_{\boldsymbol{k}}(\cdot) \approx \frac{1}{4\pi^2}\int_0^{2\pi} d\theta \int_0^{\infty} d\omega D(\omega) f_{\boldsymbol{k}}(\cdot). \tag{A6}$$

That is, we consider isotropic material in the temperature range $T \ll T_D$, with T_D the Debye temperature. In the following we derive results for the number, energy, momentum, and their corresponding fluxes in the zeroth order, for the linear and quadratic modes separately. Based on this, a generalized Euler equation is obtained.

a. Number density

We start from the number density, which is obtained by summing over all the allowed wave vectors. The mode dispersion matters in the summation. Straightforward calculation then yields

$$n_L^{(0)} = \frac{\pi}{12}(1-\tilde{u}^2)^{-3/2}(\hbar v_g\beta)^{-2}, \tag{A7a}$$

$$n_N^{(0)} = -\frac{1}{4\pi}\ln(1-\lambda')(\hbar\beta a)^{-1}. \tag{A7b}$$

Here the superscript (0) means zeroth order, $\tilde{\mathbf{u}} = \boldsymbol{u}/v_g$ is the reduced velocity, and $\lambda' = \exp(\beta\mu')$ with $\mu' = m^*u^2/2$ is the effective chemical potential due to the drift motion.

We find that, in both cases, nonzero $\boldsymbol{u}$ gives rises to correction of the quasiparticle density, which is even order in u. For linear mode we get an extra factor $(1-\tilde{u}^2)^{-3/2}$, which resembles that of the relativistic particles, with the velocity of light replaced by the group velocity of phonon quasiparticle. For the quadratic mode, the correction comes from the effective change of the chemical potential μ' due to the drift motion.

Actually, this form of $n_N^{(0)}$ should be taken with caution. In the limit of $u \to 0$, $n_N^{(0)}$ diverges logarithmically. The reason behind this result is simple. The quadratic flexural phonons have a constant density of states in the long wavelength limit. A singularity appears at k where the Bose-Einstein distribution diverges, leading to divergent $n_N^{(0)}$. One more difficulty is that, when $\mu' > 0$, phonons with $\hbar\omega_k < \mu'$ have a unphysical negative population, meaning that these phonon modes cannot be properly taken into account within the present kinetic theory. This kind of difficulty does not appear for linear phonon modes. We will discuss the consequence of divergent $n_N^{(0)}$. Meanwhile, we still use this formal result of Eq. (A7b) for the expressions of other quantities.

The above results of phonon number density shows the important difference between phonon quasiparticles and real particles with number conservation. Since phonons simply represent thermal excitation of the system, their number is not conserved.

b. Energy density and flux

Following a similar procedure, the zeroth order energy density can be obtained:

$$E_L^{(0)} = \frac{1}{2\pi}\mathrm{Li}_3(\lambda)(2+\tilde{u}^2)(1-\tilde{u}^2)^{-\frac{5}{2}}(\hbar v_g)^{-2}(k_BT)^3, \quad \text{(A8a)}$$

$$E_N^{(0)} = E_{N,U}^{(0)} + E_{N,K}^{(0)} = \frac{1}{4\pi}\mathrm{Li}_2(\lambda')(\hbar a)^{-1}(k_BT)^2 + \frac{1}{2}\rho_N^{(0)}u^2, \quad \text{(A8b)}$$

with $\rho_N^{(0)} = m^* n_N^{(0)}$, $\zeta(x)$ is the Riemann zeta function. We have split E_N into two terms $E_{N,U}^{(0)}$ and $E_{N,K}^{(0)}$. Their physical meaning is clear. The first term $E_{N,U}^{(0)}$ has the same form as the energy density in thermal equilibrium, except now $\lambda' > 1$ has an implicit u dependence. The second term $E_{N,K}^{(0)}$ is a drift correction due to the collective motion of all the phonons with the same velocity $\boldsymbol{u}$. Although $n_N^{(0)}$ itself diverges logarithmically when $u \to 0$, $E_{N,K}^{(0)}$ instead goes to zero due to the presence of an extra u^2.

At this point, it is convenient to introduce

$$W_L^{(0)} \equiv 3(1-\tilde{u}^2)^{-1}P_L^{(0)}, \quad \text{(A9a)}$$

$$W_N^{(0)} \equiv 2P_N^{(0)} + \tfrac{1}{2}\rho_N^{(0)}u^2, \quad \text{(A9b)}$$

with

$$P_L^{(0)} = \frac{1}{2\pi}\mathrm{Li}_3(\lambda)(\hbar v_g)^{-2}(1-\tilde{u}^2)^{-3/2}(k_BT)^3, \quad \text{(A10a)}$$

$$P_N^{(0)} = \frac{1}{4\pi}\mathrm{Li}_2(\lambda')(\hbar a)^{-1}(k_BT)^2. \quad \text{(A10b)}$$

$W^{(0)}$ and $P^{(0)}$ can be thought as the enthalpy density and pressure of the phonon gas, evaluated from the drifted Bose-Einstein distribution function [Eq. (A5)]. From this we can write the energy density in a different form

$$E_L^{(0)} = \frac{2+\tilde{u}^2}{1-\tilde{u}^2}P_L^{(0)}, \quad \text{(A11a)}$$

$$E_N^{(0)} = P_N^{(0)} + \tfrac{1}{2}\rho_N^{(0)}u^2. \quad \text{(A11b)}$$

The phonon energy flux is then written in a compact form

$$\boldsymbol{q}_i^{(0)} = W_i^{(0)}\boldsymbol{u}, \quad \text{(A12)}$$

which is applicable to both linear and quadratic modes.

c. Momentum density and flux

The momentum density of linear and quadratic modes takes quite different forms

$$\boldsymbol{p}_L = v_g^{-2}\boldsymbol{q}_L, \quad \text{(A13a)}$$

$$\boldsymbol{p}_N^{(0)} = \rho_N^{(0)}\boldsymbol{u}. \quad \text{(A13b)}$$

The linear dispersion leads to a general relationship between $\boldsymbol{p}_L$ and $\boldsymbol{q}_L$, Eq. (A13a), which is obtained from their definition and holds to all (quasi-)particles with linear dispersion. In the derivation of the Guyer-Krumhansl equation within the Debye model, this relationship plays a key role in relating the momentum density with the heat flux [59]. However, there is no such relationship between $\boldsymbol{p}_N$ and $\boldsymbol{q}_N$ [36]. Instead, Eq. (A13b) takes a same form as the traditional nonrelativistic gas. It shows that the momentum density is simply the drift momentum $m^*\boldsymbol{u}$ times the number density $n_N^{(0)}$. Similar to $E_N^{(0)}$, $\boldsymbol{p}_N^{(0)} \to 0$ when $\boldsymbol{u} \to 0$. If we define an effective mass density for the linear mode

$$\rho_L^{(0)} \equiv v_g^{-2}W_L^{(0)}, \quad \text{(A14)}$$

$\boldsymbol{p}_L^{(0)}$ and $\boldsymbol{p}_N^{(0)}$ can be written in the same form. Consequently, the momentum flux is written in a unified form

$$\Phi_{i,mn}^{(0)} = P_i^{(0)}\delta_{mn} + \rho_i^{(0)}u_m u_n. \quad \text{(A15)}$$

d. The generalized Euler equation

Substituting the momentum flux Eq. (A15) into its balance equation, we arrive at

$$(\partial_t + \boldsymbol{u}\cdot\nabla)\boldsymbol{u} + (\nabla\cdot\boldsymbol{u})\boldsymbol{u} + \nabla P^{(0)}/\rho^{(0)} = -\left\langle\tau_R^{-1}\right\rangle_p\boldsymbol{u}. \quad \text{(A16)}$$

Equation (A16) is the generalized Euler equation for phonons, where the driving force is $\nabla P^{(0)}$. Here $\rho^{(0)}$ without subindex represents the total "mass" density, similarly for other physical quantities. In the analysis of second sound, we will keep only the linear-in-u terms in the equations. Similarly, substituting Eq. (A12) into Eq. (4), we obtain the energy balance equation for both types of modes

$$\frac{\partial E^{(0)}}{\partial t} + \nabla\cdot(W^{(0)}\boldsymbol{u}) = 0. \quad \text{(A17)}$$

e. Comparison to standard relativistic and nonrelativistic hydrodynamics

In the above subsections we have written our results for the linear and quadratic phonons in similar forms as those of the standard relativistic and nonrelativistic hydrodynamic equations [61], respectively. Especially, the energy, momentum density and their corresponding fluxes [Eqs. (A11a)–(A15)] take the standard form. However, they do have one important difference. Here, all quantities with superscript (0) represent results obtained from the drifted Bose-Einstein distribution function [Eq. (A5)], instead of the equilibrium one as in standard hydrodynamics. Thus, strictly speaking, the linear and quadratic phonons do not fulfill the Lorentz or Galilean invariance. This has been discussed in the context of relativistic hydrodynamics of electrons in graphene [54]. However, when considering second sound propagation, we will keep only the linear-in-u terms. In that case, the quantities with superscript (0) are obtained from the equilibrium Bose-Einstein distribution, and the Lorentz and Galilean invariance are recovered for the linear and quadratic phonons, respectively.

3. Transport coefficients and dissipation

The obtained generalized Euler equation does not include any internal dissipation due to N scattering. They are included in the higher order corrections. In Appendix B we give detailed derivation based on kinetic theory up to the first order in the small parameter

$$\varepsilon_{i\boldsymbol{k}} = \tau_{N,i\boldsymbol{k}}/\tau_{R,i\boldsymbol{k}}. \quad \text{(A18)}$$

Here we follow the general phenomenology, and write the momentum flux $\Phi^{(1)}_{mn}$ into the following form:

$$\Phi^{(1)}_{mn} = -\eta\left(\partial_{x_n}u_m + \partial_{x_m}u_n - \frac{2}{D}\delta_{mn}\partial_{x_i}u_i\right) - \xi\,\delta_{mn}\partial_{x_i}u_i, \tag{A19}$$

with D the system dimension ($D = 2$ here), η and ξ the shear and bulk viscosity, respectively. The corresponding momentum balance equation including dissipation takes the general form

$$\begin{aligned}&(\partial_t + \boldsymbol{u}\cdot\boldsymbol{\nabla})\boldsymbol{u} + (\boldsymbol{\nabla}\cdot\boldsymbol{u})\boldsymbol{u} + \boldsymbol{\nabla}P/\rho^{(0)}\\ &\quad= \eta/\rho^{(0)}\nabla^2\boldsymbol{u} + \left[\left(1-\frac{2}{D}\right)\eta + \xi\right]/\rho^{(0)}\boldsymbol{\nabla}(\boldsymbol{\nabla}\cdot\boldsymbol{u})\\ &\qquad- \left\langle\tau_R^{-1}\right\rangle_p\boldsymbol{u}.\end{aligned} \tag{A20}$$

We will derive the viscosity coefficients η and ξ [Eqs. (B8a) and (B8b)] in Appendix B.

4. Energy flux equation and thermal conductivity

The energy flux balance equation can be obtained by multiplying $\hbar\omega_{i\boldsymbol{k}}\boldsymbol{v}_{i\boldsymbol{k}}\tau_{c,i\boldsymbol{k}}$ with Eq. (1) and performing the summation over $i\boldsymbol{k}$,

$$\begin{aligned}&\partial_t\sum_{i\boldsymbol{k}}(1-\chi_{i\boldsymbol{k}})\tau_{R,i\boldsymbol{k}}\boldsymbol{q}_{i\boldsymbol{k}} + \boldsymbol{q}\\ &\quad= \sum_{i\boldsymbol{k}}\chi_{i\boldsymbol{k}}\boldsymbol{q}^{(0)}_{i\boldsymbol{k}} - \sum_{i\boldsymbol{k}}(1-\chi_{i\boldsymbol{k}})\partial_T f_{i\boldsymbol{k}}\tau_{R,i\boldsymbol{k}}\hbar\omega_{i\boldsymbol{k}}\boldsymbol{v}_{i\boldsymbol{k}}\boldsymbol{v}_{i\boldsymbol{k}}\cdot\boldsymbol{\nabla}T.\end{aligned} \tag{A21}$$

The combined relaxation time is defined as

$$\tau^{-1}_{c,i\boldsymbol{k}} = \tau^{-1}_{N,i\boldsymbol{k}} + \tau^{-1}_{R,i\boldsymbol{k}}. \tag{A22}$$

It shows that the total energy current includes two contributions: one due to the collective phonon drift motion, and the other due to the temperature gradient. Their relative contributions are weighted by two factors $\chi_{i\boldsymbol{k}} = (1+\varepsilon_{i\boldsymbol{k}})^{-1}$ and $1-\chi_{i\boldsymbol{k}}$, respectively. This equation is valid in the full range of $\varepsilon_{i\boldsymbol{k}}$ and can be expanded over $\varepsilon_{i\boldsymbol{k}}$ in the hydrodynamic regime when $\varepsilon_{i\boldsymbol{k}} \ll 1$. The zeroth order result gives the null result $\boldsymbol{q}^{(0)} = \boldsymbol{q}^{(0)}$, while the first order equation is exactly Eq. (B9). To proceed, we write Eq. (A21) into a compact form

$$\langle\tau_c\rangle_q\partial_t\boldsymbol{q} + \boldsymbol{q} = \chi W^{(0)}\boldsymbol{u} - \boldsymbol{\kappa}\cdot\boldsymbol{\nabla}T. \tag{A23}$$

We have introduced an averaged characteristic relaxation time of $\boldsymbol{q}$,

$$\langle\tau_c\rangle_q = \frac{\sum_{i\boldsymbol{k}}\frac{\varepsilon_{i\boldsymbol{k}}}{1+\varepsilon_{i\boldsymbol{k}}}\tau_{R,i\boldsymbol{k}}\boldsymbol{q}_{i\boldsymbol{k}}}{\sum_{i\boldsymbol{k}}\boldsymbol{q}_{i\boldsymbol{k}}} \approx \frac{\sum_{i\boldsymbol{k}}\frac{\varepsilon_{i\boldsymbol{k}}}{1+\varepsilon_{i\boldsymbol{k}}}\tau_{R,i\boldsymbol{k}}\boldsymbol{q}^{(0)}_{i\boldsymbol{k}}}{\sum_{i\boldsymbol{k}}\boldsymbol{q}^{(0)}_{i\boldsymbol{k}}}, \tag{A24}$$

the averaged quantities

$$\chi = \frac{\sum_{i\boldsymbol{k}}\boldsymbol{q}^{(0)}_{i\boldsymbol{k}}(1+\varepsilon_{i\boldsymbol{k}})^{-1}}{\sum_{i\boldsymbol{k}}\boldsymbol{q}^{(0)}_{i\boldsymbol{k}}}, \tag{A25}$$

thermal conductivity from relaxation time approximation

$$\begin{aligned}\kappa &= L^{-2}\sum_{i\boldsymbol{k}}\hbar\omega_{i\boldsymbol{k}}v_{i\boldsymbol{k}}v_{i\boldsymbol{k}}\tau_{c,i\boldsymbol{k}}\partial_T f_{i\boldsymbol{k}}\\ &\equiv L^{-2}\sum_{i\boldsymbol{k}}\hbar\omega_{i\boldsymbol{k}}v_{i\boldsymbol{k}}v_{i\boldsymbol{k}}\langle\tau_c\rangle_\kappa\partial_T f_{i\boldsymbol{k}},\end{aligned} \tag{A26}$$

where the second equality defines an average relaxation time $\langle\tau_c\rangle_\kappa$. We note that, due to the $i\boldsymbol{k}$ dependence of $\tau_{c,i\boldsymbol{k}}$, the two averages $\langle\tau_c\rangle_\kappa$ and $\langle\tau_c\rangle_q$ are different.

APPENDIX B: DERIVATION OF THE TRANSPORT COEFFICIENTS

To consider dissipation in the hydrodynamic equations, we need to include the first order correction. By performing an expansion over $\varepsilon_{i\boldsymbol{k}}$, the first order correction to distribution function is [59]

$$\begin{aligned}f^{(1)} &= \varepsilon(f_R - f_N) - \tau_N(\partial_t f_N + \boldsymbol{v}\cdot\boldsymbol{\nabla}f_N)\\ &= \varepsilon(f_R - f_N) - \tau_N[\partial_T f_N(\partial_t T + \boldsymbol{v}\cdot\boldsymbol{\nabla}T)\\ &\quad- \partial_{\hbar\omega}f_N(\hbar\boldsymbol{k}\cdot\partial_t\boldsymbol{u} + \boldsymbol{v}\cdot(\hbar\boldsymbol{k}\cdot\boldsymbol{\nabla})\boldsymbol{u})].\end{aligned} \tag{B1}$$

The corresponding first order corrections to the momentum and energy flux are

$$\Phi^{(1)}_{mn} = \sum_{i\boldsymbol{k}}\hbar k_m v_{i\boldsymbol{k},n}f^{(1)}_{i\boldsymbol{k}}, \tag{B2}$$

$$q^{(1)}_n = \sum_{i\boldsymbol{k}}\hbar\omega_{i\boldsymbol{k}}v_{i\boldsymbol{k},n}f^{(1)}_{i\boldsymbol{k}}. \tag{B3}$$

In principle we can divide $f^{(1)}$ into even and odd (in $\boldsymbol{k}$) contributions. They contribute to $\boldsymbol{\Phi}^{(1)}$ and $\boldsymbol{q}^{(1)}$, respectively. The full evaluation of $\boldsymbol{\Phi}^{(1)}$ and $\boldsymbol{q}^{(1)}$ using Eq. (B1) is quite cumbersome. Here, as in traditional hydrodynamics, we only consider terms that are first order in $\boldsymbol{u}$ and the deviations δu, δT. The distribution function can then be split into odd ($f^{(1)}_o$) and even ($f^{(1)}_e$) parts

$$f^{(1)} \approx f^{(1)}_e + f^{(1)}_o, \tag{B4}$$

where

$$f^{(1)}_e = \tau_{N,i\boldsymbol{k}}[\partial_{\hbar\omega}f_R\hbar\boldsymbol{k}\cdot(\boldsymbol{v}\cdot\boldsymbol{\nabla})\boldsymbol{u} - \partial_T f_R\partial_t T], \tag{B5}$$

$$\begin{aligned}f^{(1)}_o &= \varepsilon_{i\boldsymbol{k}}\partial_{\hbar\omega}f_R\hbar\boldsymbol{k}\cdot\boldsymbol{u} + \tau_{N,i\boldsymbol{k}}\partial_{\hbar\omega}f_R\\ &\quad\times(\hbar\boldsymbol{k}\cdot\partial_t\boldsymbol{u} - \boldsymbol{v}\cdot\boldsymbol{\nabla}T).\end{aligned} \tag{B6}$$

1. Momentum flux

The momentum flux is obtained from $f^{(1)}_e$ as

$$\begin{aligned}\Phi^{(1)}_{mn} &= -\frac{1}{2}\sum_{i\boldsymbol{k}}\tau_{N,i\boldsymbol{k}}\alpha_i W^{(0)}_{i\boldsymbol{k}}\partial_{x_i}u_j\\ &\quad\times(\delta_{ij}\delta_{mn} + \delta_{im}\delta_{nj} + \delta_{in}\delta_{mj}) - \sum_{i\boldsymbol{k}}\tau_{N,i\boldsymbol{k}}\alpha_i C^{(0)}_{i\boldsymbol{k}}\partial_t T\delta_{mn}\\ &\equiv -\frac{1}{4}\langle\tau_N\rangle_\Phi\left(W^{(0)}_L + 2W^{(0)}_N\right)\partial_{x_i}u_j\\ &\quad\times(\delta_{ij}\delta_{mn} + \delta_{im}\delta_{nj} + \delta_{in}\delta_{mj})\\ &\quad-\frac{1}{2}\langle\tau_N\rangle_\Phi\partial_T\left(E^{(0)}_L + 2E^{(0)}_N\right)\partial_t T\delta_{mn},\end{aligned} \tag{B7}$$

Here $C_{ik}^{(0)}$, $W_{ik}^{(0)}$ are the mode resolved heat capacity and enthalpy function, respectively. We have defined the average relaxation time $\langle\tau_N\rangle_\Phi$ through the second equality. Comparing with the general form of $\Phi_{mn}^{(1)}$ [Eq. (A19)], we obtain the expressions for the shear (η) and bulk (ξ) viscosity

$$\eta = \tfrac{1}{4}\langle\tau_N\rangle_\Phi\big(W_L^{(0)} + 2W_N^{(0)}\big), \tag{B8a}$$

$$\xi = \frac{1}{2}\left(\frac{1}{D} - \frac{1}{2}\right)\langle\tau_N\rangle_\Phi\big(W_L^{(0)} + 2W_N^{(0)}\big). \tag{B8b}$$

2. Energy flux

The energy flux is obtained similarly from the odd correction $f_o^{(1)}$,

$$\boldsymbol{q}^{(1)} = -\sum_{ik}\varepsilon_{ik}W_{ik}^{(0)}\boldsymbol{u} - \sum_{ik}\tau_{N,ik}W_{ik}^{(0)}\partial_t\boldsymbol{u} - \sum_{ik}\tau_{N,ik}\alpha_i\hbar\omega_{ik}\partial_T f_{R,ik}v_{ik}^2\nabla T. \tag{B9}$$

This result can also be obtained by expansion of the full expression [Eq. (A21)] to the first order in ε_{ik}. It is understood that the $u \to 0$ limit of the zeroth order quantities $W^{(0)}$ and $E^{(0)}$ in Eqs. (B7)–(B9) should be used to be consistent with the approximation used in Eqs. (B4)–(B6).

APPENDIX C: COMPARISON BETWEEN SECOND SOUND IN HELIUM II AND IN SOLIDS

Here, for completeness, we present a comparison between second sound of helium II and phonon system in solids. The first and second sound in helium II can be understood from linearized, nondissipative version of Landau's macroscopic hydrodynamic equations [78]:

$$\frac{\partial\rho}{\partial t} + \nabla\cdot\boldsymbol{j} = 0, \tag{C1}$$

$$\frac{\partial\boldsymbol{j}}{\partial t} + \nabla P = 0, \tag{C2}$$

$$\frac{\partial\rho S}{\partial t} + \rho S\nabla\cdot\boldsymbol{v}_n = 0, \tag{C3}$$

$$\frac{\partial\boldsymbol{v}_s}{\partial t} + \nabla\mu = 0. \tag{C4}$$

Here the subscripts n and s represent normal and superfluid, respectively. Equation (C1) is a result of mass conservation, with ρ the total mass density and j the mass flux or momentum density. Equation (C2) represents the conservation of momentum, with P the pressure. Equation (C3) means that the total entropy (ρS) is conserved, since we have ignored the dissipative processes. One important point is that the entropy is only carried by normal fluid, thus $\boldsymbol{v}_n$. The fourth equation is special to superfluid. It represents the potential flow (μ the chemical potential) of superfluid. Landau obtained this equation from the requirement of $\nabla\times\boldsymbol{v}_s = 0$. We now know that $\boldsymbol{v}_s \propto \nabla\Phi$, where Φ is the phase of the Bose-Einstein condensed superfluid wave function.

From Eqs. (C1) and (C2) we can get the equations of motion for $\boldsymbol{v}_n$ and $\boldsymbol{v}_s$, respectively,

$$\rho_n\frac{\partial\boldsymbol{v}_n}{\partial t} + \frac{\rho_n}{\rho}\nabla P + \rho_s S\nabla T = 0, \tag{C5}$$

$$\rho_s\frac{\partial\boldsymbol{v}_s}{\partial t} + \frac{\rho_s}{\rho}\nabla P - \rho_s S\nabla T = 0. \tag{C6}$$

We can also write them in terms of the relative velocity of the normal and superfluid $\boldsymbol{w} = \boldsymbol{v}_n - \boldsymbol{v}_s$ and obtain

$$\rho\frac{\partial S}{\partial t} + \rho_s S\nabla\cdot\boldsymbol{w} = 0, \tag{C7}$$

$$\frac{\partial\boldsymbol{w}}{\partial t} + \frac{\rho}{\rho_n}S\nabla T = 0. \tag{C8}$$

We see that the in-phase motion of the normal and superfluid couples to pressure [Eqs. (C1) and (C2)], while the out-of-phase/relative motion couples to entropy and temperature [Eqs. (C7) and (C8)]. As a result, we obtain

$$\frac{\partial^2\rho}{\partial t^2} - \nabla^2 P = 0, \tag{C9}$$

$$\frac{\partial^2 S}{\partial t^2} - \frac{\rho_s S^2}{\rho_n}\nabla^2 T = 0. \tag{C10}$$

We now show that the former group gives rise to the first sound, and the latter group gives the second sound. Writing $\rho = \rho(P,T)$ and $S = S(P,T)$ in terms of P and T, and performing a linear analysis, we get

$$\left(\frac{\partial\rho}{\partial T}\right)_P\delta T + \left(\frac{1}{v_1^2} - \frac{1}{v^2}\right)\delta P = 0, \tag{C11}$$

$$\frac{v_2^2 C}{T}\left(\frac{1}{v_2^2} - \frac{1}{v^2}\right)\delta T + \left(\frac{\partial S}{\partial P}\right)_T\delta P = 0, \tag{C12}$$

with

$$v_1 = \sqrt{\frac{\partial P}{\partial\rho}}, \quad v_2 = \sqrt{\frac{TS^2\rho_s}{C\rho_n}}. \tag{C13}$$

The condition that the above two equations have solutions gives

$$\left(1 - \frac{v_1^2}{v^2}\right)\left(1 - \frac{v_2^2}{v^2}\right) = 0. \tag{C14}$$

Here we have ignored the difference between heat capacity at constant volume and that at constant pressure. We get two sound solutions, whose velocities are given by v_1 and v_2. We recognize v_1 as velocity of the normal first sound. v_2 is then that of the second sound. Laudau showed that if we consider only phonon contribution (ignoring roton), we have $v_2 = v_1/\sqrt{3}$.

The most important point to present this analysis is to show that the existence of second sound in helium II relies on the relative out-of-phase motion of the normal and superfluid (w). Thus, second sound in helium II is a result of quantum mechanical effect, since its appearance relies on the presence of Bose-Einstein condensation.

The similarity between second sound in helium II and in solids can be explained by considering the simple Debye model with one linear phonon branch $\omega = v_g k$. We assume that the phonon system follows the drifted distribution $f_{N,ik}$

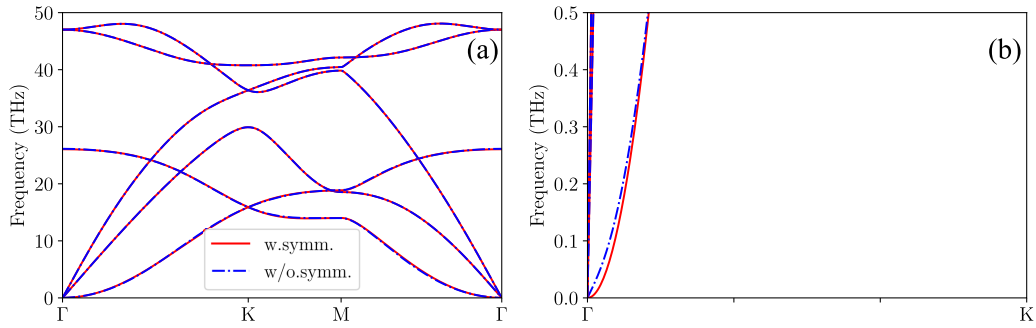

FIG. 5. (a) Phonon dispersion of graphene along high symmetry directions. (b) Zoom in of the dispersion near Γ in (a). The blue and red lines correspond to results before and after the symmetrization of the force constants, which guarantees the translational and rotational symmetry are fulfilled. The ideal quadratic dispersion of ZA mode is recovered after the symmetrization.

due to the dominant normal scattering process. In the linear-in-$\boldsymbol{u}$ limit, if we ignore all the dissipative processes, the energy flux $\boldsymbol{q}$ and the momentum density $\boldsymbol{p}$ are proportional to $\boldsymbol{u}$, with $\boldsymbol{q} = v_g^2 \boldsymbol{p} = W^{(0)}\boldsymbol{u}$. The energy balance equation then becomes

$$\frac{\partial E^{(0)}}{\partial t} + W^{(0)} \nabla \cdot \boldsymbol{u} = 0. \tag{C15}$$

We also have the momentum balance equation

$$\partial_t \boldsymbol{p} + \nabla P^{(0)} = 0 \to W^{(0)} v_g^{-2} \partial_t \boldsymbol{u} + \nabla P^{(0)} = 0. \tag{C16}$$

As discussed in Appendix A 2 e, although $W^{(0)}, E^{(0)}, P^{(0)}$ are calculated from the drifted distribution, their difference with the equilibrium value is at least second order in u. Thus, here to the lowest order, they can be taken as the equilibrium value. For D-dimensional phonon gas with linear dispersion, we have the following relations:

$$E^{(0)} = DP^{(0)}, \tag{C17}$$

$$W^{(0)} = E^{(0)} + P^{(0)} = (D+1)P^{(0)}, \tag{C18}$$

$$S^{(0)} = (D+1)P^{(0)}/T. \tag{C19}$$

Thus, we can write Eq. (C15) in another form

$$\frac{\partial S^{(0)}}{\partial t} + (1 + D^{-1}) S^{(0)} \nabla \cdot \boldsymbol{u} = 0. \tag{C20}$$

This equation can be compared with Eq. (C7). We see that the common drift velocity $\boldsymbol{u}$ plays the role of relative velocity $\boldsymbol{w}$ between the normal and superfluid in helium II. But the origin of $\boldsymbol{u}$ is the momentum conserving normal phonon scattering, which does not need to be quantum mechanical. Combining with Eqs. (C16), we get an equation for the entropy

$$\frac{\partial^2 S^{(0)}}{\partial t^2} - \frac{v_g^2}{D} \nabla^2 S^{(0)} = 0, \tag{C21}$$

which gives rises to the drifting second sound with velocity $v_p = v_g/\sqrt{D}$.

APPENDIX D: DETAILS OF THE DFT CALCULATION

Phonon dispersion relation of graphene is calculated using Vienna *ab initio* simulation package (VASP) [79,80] combined with phonopy (Fig. 5) [81]. We use a supercell size $5 \times 5 \times 1$ to calculate the second order force constants. The numerical flexural phonon dispersion does not follow the ideal quadratic relation near Γ (blue dashed-dotted line). Additional symmetrization is used to recover the quadratic dispersion (red solid line) [68]. This slight change of dispersion has important influence on the second sound dispersion (Fig. 2).

To obtain the relaxation times, we calculate the third order force constant using phono3py [82] with the same supercell size. The numbers of mesh points for reciprocal space

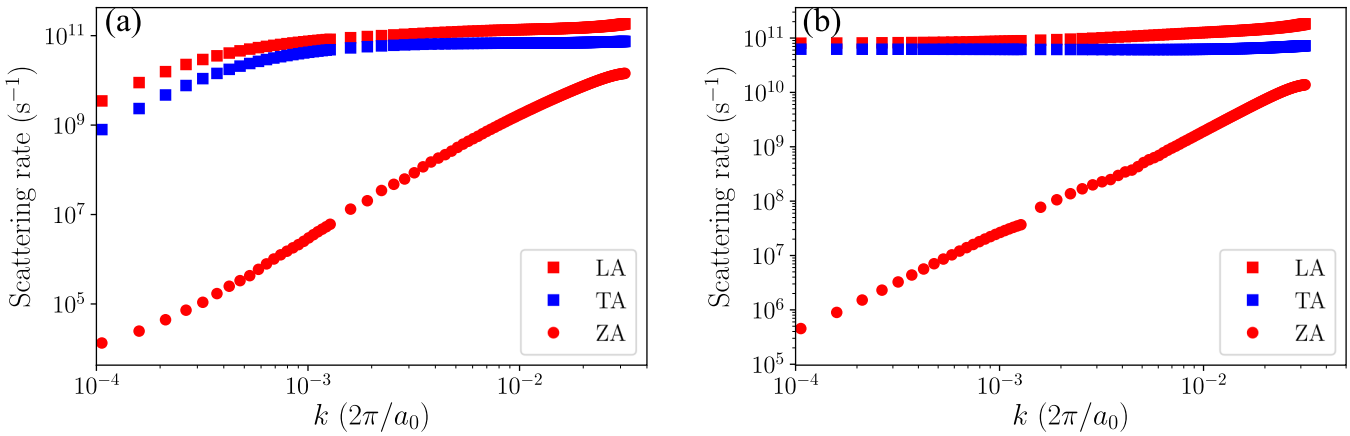

FIG. 6. The scattering rate of acoustic phonon modes for graphene at 100 K before (a) and after (b) the symmetrization. The ZA mode shows the smallest scattering due to mirror symmetry of graphene about the 2D plane.

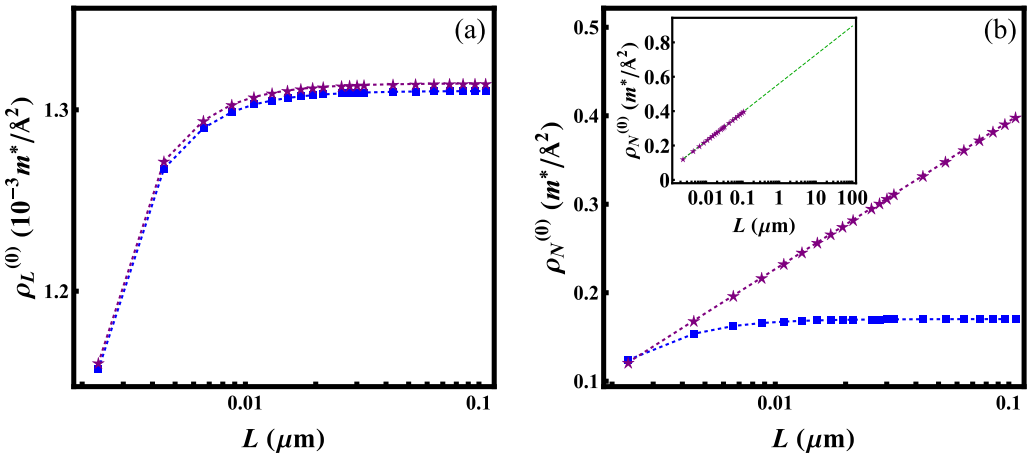

FIG. 7. Dependence of the effective mass density $\rho^{(0)}$ on the sample size for linear (a) and flexural (b) phonon modes of graphene at 100 K. Results before and after symmetrization of the forces constants are shown in blue (square) and purple (star symbols), respectively. The logarithmic dependence of $\rho_N^{(0)}$ on L is recovered after the symmetrization. Note that $\rho_L^{(0)}$ is two orders of magnitude smaller than $\rho_N^{(0)}$. The inset in (b) shows fitting of $\rho_N^{(0)}$ to $\ln L$. Extrapolation of $\rho_N^{(0)}$ to $L = 50$ μm is used in the numerical calculation of Fig. 2. $m^* = \hbar/(2a)$ is the effective mass defined in the main text.

sampling are $501 \times 501 \times 1$. The scattering rates before and after the symmetrization of graphene are shown in Fig. 6. The viscosity, thermal conductivity under relaxation time approximation and the effective mass density are obtained using these numerical results and used to calculate the second sound dispersion. As an example, we show in Fig. 7 the dependence of $\rho_L^{(0)}$ (a) and $\rho_N^{(0)}$ (b) on the sample size before and after the symmetrization.

[1] G. Chen, Non-Fourier phonon heat conduction at the microscale and nanoscale, Nat. Rev. Phys. **3**, 555 (2021).

[2] J.-S. Wang, J. Wang, and J. T. Lü, Quantum thermal transport in nanostructures, Eur. Phys. J. B **62**, 381 (2008).

[3] A. Dhar, Heat transport in low-dimensional systems, Adv. Phys. **57**, 457 (2008).

[4] N. Li, J. Ren, L. Wang, G. Zhang, P. Hänggi, and B. Li, Colloquium: Phononics: Manipulating heat flow with electronic analogs and beyond, Rev. Mod. Phys. **84**, 1045 (2012).

[5] X. Gu, Y. Wei, X. Yin, B. Li, and R. Yang, Colloquium: Phononic thermal properties of two-dimensional materials, Rev. Mod. Phys. **90**, 041002 (2018).

[6] S. Lepri, R. Livi, and A. Politi, Thermal conduction in classical low-dimensional lattices, Phys. Rep. **377**, 1 (2003).

[7] L. E. Gurevich and B. I. Shklovskii, Theory of the second sound in semiconductors, Sov. Phys. Solid State **8**, 2434 (1967).

[8] H. Nielsen and B. I. Shklovskii, Heat transfer and second sound in dielectrics at large drift velocities of the phonon gas, Sov. Phys. JETP **29**, 386 (1969).

[9] L. J. Sham, Equilibrium approach to second sound in solids, Phys. Rev. **156**, 494 (1967).

[10] L. J. Sham, Temperature propagation in anharmonic solids, Phys. Rev. **163**, 401 (1967).

[11] H. Beck, P. F. Meier, and A. Thellung, Phonon hydrodynamics in solids, Phys. Status Solidi (a) **24**, 11 (1974).

[12] D. D. Joseph and L. Preziosi, Heat waves, Rev. Mod. Phys. **61**, 41 (1989).

[13] S. Lee and X. Li, Hydrodynamic phonon transport: Past, present and prospects, in *Nanoscale Energy Transport*, 2053-2563 (IOP, London, 2020), pp. 1–1 to 1–26.

[14] J. Wang, G. Dai, and J. Huang, Thermal metamaterial: Fundamental, application, and outlook, iScience **23**, 101637 (2020).

[15] K. Nakamura, *Quantum Phononics: Introduction to Ultrafast Dynamics of Optical Phonons* (Springer, Cham, 2019).

[16] Y. Li, W. Li, T. Han, X. Zheng, J. Li, B. Li, S. Fan, and C.-W. Qiu, Transforming heat transfer with thermal metamaterials and devices, Nat. Rev. Mater. **6**, 488 (2021).

[17] J. C. Ward and J. Wilks, The velocity of second sound in liquid helium near the absolute zero, Philos. Mag. **42**, 314 (1951).

[18] J. C. Ward and J. Wilks, Second sound and the thermo-mechanical effect at very low temperatures, Philos. Mag. **43**, 48 (1952).

[19] J. A. Sussmann and A. Thellung, Thermal conductivity of perfect dielectric crystals in the absence of umklapp processes, Proc. Phys. Soc. **81**, 1122 (1963).

[20] R. N. Gurzhi, Hydrodynamic effects in solids at low temperature, Sov. Phys. Usp. **11**, 255 (1968).

[21] R. A. Guyer and J. A. Krumhansl, Solution of the linearized phonon Boltzmann equation, Phys. Rev. **148**, 766 (1966).

[22] R. A. Guyer and J. A. Krumhansl, Thermal conductivity, second sound, and phonon hydrodynamic phenomena in nonmetallic crystals, Phys. Rev. **148**, 778 (1966).

[23] R. J. Hardy, Phonon Boltzmann equation and second sound in solids, Phys. Rev. B **2**, 1193 (1970).

[24] C. C. Ackerman, B. Bertman, H. A. Fairbank, and R. A. Guyer, Second Sound in Solid Helium, Phys. Rev. Lett. **16**, 789 (1966).

[25] T. F. McNelly, S. J. Rogers, D. J. Channin, R. J. Rollefson, W. M. Goubau, G. E. Schmidt, J. A. Krumhansl, and R. O. Pohl,

Heat Pulses in NaF: Onset of Second Sound, Phys. Rev. Lett. **24**, 100 (1970).
[26] V. Narayanamurti and R. C. Dynes, Observation of Second Sound in Bismuth, Phys. Rev. Lett. **28**, 1461 (1972).
[27] A. Koreeda, R. Takanao, and S. Saikan, Second Sound in $SrTiO_3$, Phys. Rev. Lett. **99**, 265502 (2007).
[28] S. Lee, D. Broido, K. Esfarjani, and G. Chen, Hydrodynamic phonon transport in suspended graphene, Nat. Commun. **6**, 6290 (2015).
[29] A. Cepellotti, G. Fugallo, L. Paulatto, M. Lazzeri, F. Mauri, and N. Marzari, Phonon hydrodynamics in two-dimensional materials, Nat. Commun. **6**, 6400 (2015).
[30] Z. Ding, J. Zhou, B. Song, V. Chiloyan, M. Li, T.-H. Liu, and G. Chen, Phonon hydrodynamic heat conduction and Knudsen minimum in graphite, Nano Lett. **18**, 638 (2018).
[31] V. Martelli, J. L. Jiménez, M. Continentino, E. Baggio-Saitovitch, and K. Behnia, Thermal Transport and Phonon Hydrodynamics in Strontium Titanate, Phys. Rev. Lett. **120**, 125901 (2018).
[32] Y. Machida, A. Subedi, K. Akiba, A. Miyake, M. Tokunaga, Y. Akahama, K. Izawa, and K. Behnia, Observation of Poiseuille flow of phonons in black phosphorus, Sci. Adv. **4**, eaat3374 (2018).
[33] Y. Machida, N. Matsumoto, T. Isono, and K. Behnia, Phonon hydrodynamics and ultrahigh–room-temperature thermal conductivity in thin graphite, Science **367**, 309 (2020).
[34] S. Huberman, R. A. Duncan, K. Chen, B. Song, V. Chiloyan, Z. Ding, A. A. Maznev, G. Chen, and K. A. Nelson, Observation of second sound in graphite at temperatures above 100 K, Science **364**, 375 (2019).
[35] A. Cepellotti and N. Marzari, Thermal Transport in Crystals as a Kinetic Theory of Relaxons, Phys. Rev. X **6**, 041013 (2016).
[36] M.-Y. Shang, C. Zhang, Z. Guo, and J.-T. Lü, Heat vortex in hydrodynamic phonon transport of two-dimensional materials, Sci. Rep. **10**, 8272 (2020).
[37] Y. Guo and M. Wang, Heat transport in two-dimensional materials by directly solving the phonon Boltzmann equation under Callaway's dual relaxation model, Phys. Rev. B **96**, 134312 (2017).
[38] S. Lee and L. Lindsay, Hydrodynamic phonon drift and second sound in a (20,20) single-wall carbon nanotube, Phys. Rev. B **95**, 184304 (2017).
[39] X.-P. Luo, Y.-Y. Guo, M.-R. Wang, and H.-L. Yi, Direct simulation of second sound in graphene by solving the phonon Boltzmann equation via a multiscale scheme, Phys. Rev. B **100**, 155401 (2019).
[40] A. Beardo, M. G. Hennessy, L. Sendra, J. Camacho, T. G. Myers, J. Bafaluy, and F. X. Alvarez, Phonon hydrodynamics in frequency-domain thermoreflectance experiments, Phys. Rev. B **101**, 075303 (2020).
[41] P. Torres, A. Ziabari, A. Torelló, J. Bafaluy, J. Camacho, X. Cartoixó, A. Shakouri, and F. X. Alvarez, Emergence of hydrodynamic heat transport in semiconductors at the nanoscale, Phys. Rev. Materials **2**, 076001 (2018).
[42] C. Zhang, D. Ma, M. Shang, X. Wan, J.-T. Lü, Z. Guo, B. Li, and N. Yang, Graded thermal conductivity in 2D and 3D homogeneous hotspot systems, Mater. Today Phys. **22**, 100605 (2022).
[43] C. Yu, Y. Ouyang, and J. Chen, A perspective on the hydrodynamic phonon transport in two-dimensional materials, J. Appl. Phys. **130**, 010902 (2021).
[44] P. Scuracchio, K. H. Michel, and F. M. Peeters, Phonon hydrodynamics, thermal conductivity, and second sound in two-dimensional crystals, Phys. Rev. B **99**, 144303 (2019).
[45] J. Crossno, J. K. Shi, K. Wang, X. Liu, A. Harzheim, A. Lucas, S. Sachdev, P. Kim, T. Taniguchi, K. Watanabe, T. A. Ohki, and K. C. Fong, Observation of the Dirac fluid and the breakdown of the Wiedemann-Franz law in graphene, Science **351**, 1058 (2016).
[46] D. A. Bandurin, I. Torre, R. K. Kumar, M. B. Shalom, A. Tomadin, A. Principi, G. H. Auton, E. Khestanova, K. S. Novoselov, I. V. Grigorieva, L. A. Ponomarenko, A. K. Geim, and M. Polini, Negative local resistance caused by viscous electron backflow in graphene, Science **351**, 1055 (2016).
[47] P. J. W. Moll, P. Kushwaha, N. Nandi, B. Schmidt, and A. P. Mackenzie, Evidence for hydrodynamic electron flow in $PdCoO_2$, Science **351**, 1061 (2016).
[48] J. A. Sulpizio, L. Ella, A. Rozen, J. Birkbeck, D. J. Perello, D. Dutta, M. Ben-Shalom, T. Taniguchi, K. Watanabe, T. Holder, R. Queiroz, A. Principi, A. Stern, T. Scaffidi, A. K. Geim, and S. Ilani, Visualizing Poiseuille flow of hydrodynamic electrons, Nature (London) **576**, 75 (2019).
[49] P. Gallagher, C.-S. Yang, T. Lyu, F. Tian, R. Kou, H. Zhang, K. Watanabe, T. Taniguchi, and F. Wang, Quantum-critical conductivity of the Dirac fluid in graphene, Science **364**, 158 (2019).
[50] L. Ella, A. Rozen, J. Birkbeck, M. Ben-Shalom, D. Perello, J. Zultak, T. Taniguchi, K. Watanabe, A. K. Geim, S. Ilani, and J. A. Sulpizio, Simultaneous voltage and current density imaging of flowing electrons in two dimensions, Nat. Nanotechnol. **14**, 480 (2019).
[51] A. I. Berdyugin, S. G. Xu, F. M. D. Pellegrino, R. K. Kumar, A. Principi, I. Torre, M. B. Shalom, T. Taniguchi, K. Watanabe, I. V. Grigorieva, M. Polini, A. K. Geim, and D. A. Bandurin, Measuring Hall viscosity of graphene's electron fluid, Science **364**, 162 (2019).
[52] A. Levchenko and J. Schmalian, Transport properties of strongly coupled electron–phonon liquids, Ann. Phys. **419**, 168218 (2020).
[53] X. Huang and A. Lucas, Electron-phonon hydrodynamics, Phys. Rev. B **103**, 155128 (2021).
[54] B. N. Narozhny, Electronic hydrodynamics in graphene, Ann. Phys. **411**, 167979 (2019).
[55] R. J. Hardy and S. S. Jaswal, Velocity of second sound in NaF, Phys. Rev. B **3**, 4385 (1971).
[56] A. Beardo, M. López-Suárez, L. A. Pérez, L. Sendra, M. I. Alonso, C. Melis, J. Bafaluy, J. Camacho, L. Colombo, R. Rurali, F. X. Alvarez, and J. S. Reparaz, Observation of second sound in a rapidly varying temperature field in Ge, Sci. Adv. **7**, eabg4677(2021).
[57] M. Simoncelli, N. Marzari, and A. Cepellotti, Generalization of Fourier's Law into Viscous Heat Equations, Phys. Rev. X **10**, 011019 (2020).
[58] J. Callaway, Model for lattice thermal conductivity at low temperatures, Phys. Rev. **113**, 1046 (1959).
[59] Y. Guo and M. Wang, Phonon hydrodynamics and its applications in nanoscale heat transport, Phys. Rep. **595**, 1 (2015).

[60] These expressions hold in the constant relaxation time approximation, i.e., $\langle\tau_c\rangle_\kappa = \langle\tau_c\rangle_q = \langle\tau_c\rangle$.
[61] L. D. Landau and E. M. Lifshitz, *Fluid Mechanics*, 2nd ed. (Pergamon, New York, 1987).
[62] S. G. Volz, Thermal Insulating Behavior in Crystals at High Frequencies, Phys. Rev. Lett. **87**, 074301 (2001).
[63] L. Chaput, Direct Solution to the Linearized Phonon Boltzmann Equation, Phys. Rev. Lett. **110**, 265506 (2013).
[64] C. Hua and L. Lindsay, Space-time dependent thermal conductivity in nonlocal thermal transport, Phys. Rev. B **102**, 104310 (2020).
[65] Y. K. Koh and D. G. Cahill, Frequency dependence of the thermal conductivity of semiconductor alloys, Phys. Rev. B **76**, 075207 (2007).
[66] E. Mariani and F. von Oppen, Flexural Phonons in Free-Standing Graphene, Phys. Rev. Lett. **100**, 076801 (2008).
[67] U. Aseginolaza, T. Cea, R. Bianco, L. Monacelli, M. Calandra, A. Bergara, F. Mauri, and I. Errea, Bending rigidity and sound propagation in graphene, arXiv:2005.12047.
[68] J. Carrete, W. Li, L. Lindsay, D. A. Broido, L. J. Gallego, and N. Mingo, Physically founded phonon dispersions of few-layer materials and the case of borophene, Mater. Res. Lett. **4**, 204 (2016).
[69] Z. Zhang, Y. Ouyang, Y. Guo, T. Nakayama, M. Nomura, S. Volz, and J. Chen, Hydrodynamic phonon transport in bulk crystalline polymers, Phys. Rev. B **102**, 195302 (2020).
[70] L. F. C. Pereira and D. Donadio, Divergence of the thermal conductivity in uniaxially strained graphene, Phys. Rev. B **87**, 125424 (2013).
[71] N. Bonini, J. Garg, and N. Marzari, Acoustic phonon lifetimes and thermal transport in free-standing and strained graphene, Nano Lett. **12**, 2673 (2012).
[72] L. Lindsay, W. Li, J. Carrete, N. Mingo, D. A. Broido, and T. L. Reinecke, Phonon thermal transport in strained and unstrained graphene from first principles, Phys. Rev. B **89**, 155426 (2014).
[73] G. Fugallo, A. Cepellotti, L. Paulatto, M. Lazzeri, N. Marzari, and F. Mauri, Thermal conductivity of graphene and graphite: Collective excitations and mean free paths, Nano Lett. **14**, 6109 (2014).
[74] Y. Kuang, L. Lindsay, and B. Huang, Unusual enhancement in intrinsic thermal conductivity of multilayer graphene by tensile strains, Nano Lett. **15**, 6121 (2015).
[75] Y. Kuang, L. Lindsay, S. Shi, X. Wang, and B. Huang, Thermal conductivity of graphene mediated by strain and size, Int. J. Heat Mass Transf. **101**, 772 (2016).
[76] X. Gu and R. Yang, First-principles prediction of phononic thermal conductivity of silicene: A comparison with graphene, J. Appl. Phys. **117**, 025102 (2015).
[77] X. Xu, L. F. C. Pereira, Y. Wang, J. Wu, K. Zhang, X. Zhao, S. Bae, C. Tinh Bui, R. Xie, J. T. L. Thong, B. H. Hong, K. P. Loh, D. Donadio, B. Li, and B. Özyilmaz, Length-dependent thermal conductivity in suspended single-layer graphene, Nat. Commun. **5**, 3689 (2014).
[78] L. Landau, Two-fluid model of liquid helium II, J. Phys. USSR **5**, 71 (1941).
[79] G. Kresse and J. Furthmüller, Efficient iterative schemes for *ab initio* total-energy calculations using a plane-wave basis set, Phys. Rev. B **54**, 11169 (1996).
[80] G. Kresse and J. Furthmüller, Efficiency of ab-initio total energy calculations for metals and semiconductors using a plane-wave basis set, Comput. Mater. Sci. **6**, 15 (1996).
[81] A. Togo and I. Tanaka, First principles phonon calculations in materials science, Scr. Mater. **108**, 1 (2015).
[82] A. Togo, L. Chaput, and I. Tanaka, Distributions of phonon lifetimes in Brillouin zones, Phys. Rev. B **91**, 094306 (2015).